UC Berkeley

UC Berkeley Previously Published Works

Title

Characteristics and Variability of Winter Northern Pacific Atmospheric River Flavors

Permalink

https://escholarship.org/uc/item/5rh7q6js

Journal

Journal of Geophysical Research: Atmospheres, 127(23)

ISSN

2169-897X

Authors

Zhou, Yang

O'Brien, Travis A

Collins, William D

et al.

Publication Date

2022-12-16

DOI

10.1029/2022jd037105

Copyright Information

This work is made available under the terms of a Creative Commons Attribution License, available at https://creativecommons.org/licenses/by/4.0/

Peer reviewed

eScholarship.org Powered by the California Digital Library
University of California

Check for updates

JGR Atmospheres

RESEARCH ARTICLE
10.1029/2022JD037105

Special Section:
Atmospheric Rivers: Intersection of Weather and Climate

Characteristics and Variability of Winter Northern Pacific Atmospheric River Flavors

Yang Zhou[1], Travis A. O'Brien[1,2], William D. Collins[1,3], Christine A. Shields[4], Burlen Loring[5], and Abdelrahman A. Elbashandy[5]

[1]Climate and Ecosystem Sciences Division, Lawrence Berkeley National Laboratory, Berkeley, CA, USA, [2]Department of Earth and Atmospheric Sciences, Indiana University, Bloomington, IN, USA, [3]University of California, Berkeley, Berkeley, CA, USA, [4]National Center for Atmospheric Research, Boulder, CO, USA, [5]Computational Sciences Division, Lawrence Berkeley National Laboratory, Berkeley, CA, USA

Abstract Atmospheric rivers (ARs) are intensive poleward moisture transport events that are essential to the global hydrological cycle and are often linked to extreme weather events. We categorize the winter North Pacific ARs into two "flavors": wind-dominated (windy ARs) and moisture-dominated (wet ARs) using 40 years of hourly data from fifth generation of the European Centre for Medium-Range Weather Forecasts Interim Reanalysis. We compare the differences between windy ARs and wet ARs including the lifecycle characteristics (such as genesis locations and changes of meteorological elements through the lifecycle), overall AR frequency, landfall impacts, and variability. The windy ARs are more likely to occur in the midlatitudes, while wet ARs are more active in the subtropics. Windy ARs are associated with intensive surface pressure lows, where the strong pressure gradient can support the strong wind within ARs. Due to larger size and longer lifetime, wet ARs are more likely to produce more precipitation over a lifecycle. By scaling the landfalling ARs, we show that wet ARs dominate the high-category ARs (Category 4 and 5) with higher spatial frequency and more precipitation, and windy ARs have higher contributions in the lower AR categories especially over British Columbia. Windy ARs are modulated by El Niño Southern Oscillation (ENSO) teleconnections via the anomalous geopotential height and extended subtropical jet. Wet ARs are affected by the anomalous sea surface temperature over the midlatitudes related to ENSO. Sensitivity analysis with an alternate AR detection algorithm shows consistent results on AR flavors but with disagreement on the amplitude.

Plain Language Summary Atmospheric rivers (ARs) are long and narrow plumes in the atmosphere that transport water vapor from the tropics to high latitudes. ARs generally have strong wind and rich moisture, but the relative strength of wind and moisture can be different for individual ARs. This study divides the ARs into two flavors: windy ARs (stronger wind and less moisture) and wet ARs (weaker wind and more moisture) and compares the differences within. Results show that windy ARs are more likely to occur in the midlatitudes and make landfall in British Columbia. Wet ARs are more active over the subtropics and more prevalent over the U.S. West Coast, especially in California. Windy ARs and wet ARs respond differently to climate variability like El Niño Southern Oscillation. This study could help us to understand the processes related to AR lifecycles and their variability, and help to address how ARs will change in the future warming climate.

Key Points:

- Different atmospheric river (AR) flavors have distinct lifecycle characteristics including genesis, development, and landfall impacts
- Wet ARs are more associated with the U.S. West Coast precipitation and windy ARs are more active over British Columbia
- The two AR flavors respond differently to El Niño Southern Oscillation phases

Supporting Information:

Supporting Information may be found in the online version of this article.

Correspondence to:

Y. Zhou,
yzhou2@lbl.gov

Citation:

Zhou, Y., O'Brien, T. A., Collins, W. D., Shields, C. A., Loring, B., & Elbashandy, A. A. (2022). Characteristics and variability of winter northern Pacific atmospheric river flavors. *Journal of Geophysical Research: Atmospheres*, *127*, e2022JD037105. https://doi.org/10.1029/2022JD037105

Received 12 MAY 2022
Accepted 9 NOV 2022

Author Contributions:

Conceptualization: Yang Zhou, Travis A. O'Brien, William D. Collins
Data curation: Yang Zhou
Formal analysis: Yang Zhou
Funding acquisition: William D. Collins
Investigation: Yang Zhou
Methodology: Yang Zhou, Travis A. O'Brien, William D. Collins, Christine A. Shields

© 2022 Lawrence Berkeley National Laboratory and The Authors.
This is an open access article under the terms of the Creative Commons Attribution License, which permits use, distribution and reproduction in any medium, provided the original work is properly cited.

1. Introduction

Atmospheric rivers (ARs) are narrow plumes of poleward moisture transport that have close connections to weather and climate extremes (Neiman et al., 2008; Ralph et al., 2004). ARs play a key role in the global hydrological cycle (Nash et al., 2018; Newell et al., 1992; Zhu & Newell, 1994). In recent decades, the number of AR-related studies has increased rapidly, which indicates that the scientific interest in ARs has grown quickly in studies related to regional and global extremes and hydroclimate (Ralph et al., 2017). ARs are characterized by high water vapor content and strong wind and usually occur ahead of cold fronts associated with mid-latitude storms (Bao et al., 2006; Cordeira et al., 2013; Ralph et al., 2005). They are important sources of water resources in coastal regions due to the precipitation caused by orographic lifting when ARs make landfall (Dettinger, 2013; Dettinger et al., 2011; Gershunov et al., 2017; Lavers & Villarini, 2015; Lavers et al., 2012). Over the U.S. West Coast, about 30%–50% of winter precipitation is sourced from landfalling ARs (Dettinger et al., 2011; Gershunov et al., 2017; Guan et al., 2010, 2013; J. Kim et al., 2013). ARs are also associated with heavy precipitation and

Project Administration: William D. Collins
Resources: Travis A. O'Brien
Software: Travis A. O'Brien, Burlen Loring, Abdelrahman A. Elbashandy
Supervision: Travis A. O'Brien, William D. Collins
Validation: Yang Zhou
Visualization: Yang Zhou
Writing – original draft: Yang Zhou
Writing – review & editing: Yang Zhou, Travis A. O'Brien, William D. Collins, Christine A. Shields, Burlen Loring

can cause hazardous impacts like floods and landslides (Dettinger et al., 2011; Lavers et al., 2011; Neiman et al., 2013). Waliser and Guan (2017) showed that 40%–75% of extreme wind and precipitation over 40% of the world's coastline. Because ARs can be either beneficial or hazardous to natural resources, infrastructure, and human activity, a better understanding of the characteristics and development of ARs including the relative contributions from the dynamic and thermodynamic processes is necessary.

Generally, ARs are identified by the column-integrated vapor transport (IVT) which is the magnitude of the vertically integrated product of wind and moisture. Indeed, moisture is essential to ARs because it maintains the status of ARs and supports precipitation (Dacre et al., 2015). The moisture sources of ARs include the local moisture convergence, moisture carried by the mean wind, and direct transport from the tropics (Bao et al., 2006; Knippertz & Wernli, 2010; Sodemann & Stohl, 2013). Besides the importance of moisture, an increasing number of studies emphasize the importance of wind–both horizontal and vertical–in the precipitation resulting from ARs. By analyzing landfalling ARs over Alaska, Papineau and Holloway (2011) show that ARs with rich moisture cannot produce a large amount of precipitation due to a lack of dynamical forcing. Besides, studies highlight the role of the low-level jet in AR-related precipitation (Hu & Dominguez, 2019; Smith et al., 2010). Zavadoff and Kirtman (2020) compare the dynamic and thermodynamic modulators of ARs and conclude that although ARs depend on the atmospheric moisture availability, the intensity, structure, and variability of ARs are largely modulated by dynamic processes such as Rossby wave breaking and the modulation of the jet stream. Additionally, Oueslati et al. (2019) conducted a case study and find that vertical motion has the most dominant contribution to AR-related extreme precipitation. Studies also investigated how the changes in wind and moisture by climate variability (such as El Niño Southern Oscillation [ENSO]) can affect AR activity. Research shows that during El Niño, the AR activity over the Northeast Pacific is significantly increased (Guan & Waliser, 2015; Mundhenk et al., 2016; Payne & Magnusdottir, 2014), which is associated with the extended subtropical jet and the deepened Aleutian Low (H. Kim et al., 2017; Xiong & Ren, 2021). Besides, the increased AR activity during El Niño is also attributed to enhanced cyclonic wave breaking activity that is facilitated by the extended jet (Ryoo et al., 2013). Given that an increasing trend in AR frequency is demonstrated in climate projection models (Dettinger, 2011; Espinoza et al., 2018; Lavers et al., 2013; Warner et al., 2015), numerous studies have focused on attributing future changes in ARs to contributions from changes in large-scale circulation (dynamic forcing) and changes in atmospheric moisture content due to the rising temperature (thermodynamic forcing). Overall, studies suggest both the dynamic and thermodynamic effects are important for future AR changes, to extents that vary seasonally and geographically (Gao et al., 2015; Lavers et al., 2013; McClenny et al., 2020; Payne & Magnusdottir, 2015).

The aforementioned literature demonstrates the complexity in quantifying the relative importance of dynamic and thermodynamic processes—wind versus moisture—in ARs and how they contribute to AR precipitation. Due to the large variance in wind and moisture profiles, ARs can have different characteristics, or "flavors," which will lead to different precipitation and other landfall impacts. A recent study by Gonzales et al. (2020) categorizes the U.S. West Coast landfalling ARs into "wind-dominated" and "moisture-dominated" flavors and shows that wind-dominated ARs can produce more daily precipitation at a given IVT. They also demonstrated an increasing trend in the moisture-dominated ARs in the observational record. However, Gonzales et al. (2020) is limited by only focusing on landfalling ARs and their impacts over land. How the relative dominance of wind and moisture will change through the lifecycle of ARs remains unanswered. Previous studies showed that landfalling ARs in different regions have various impact levels and distinct characteristics including genesis locations and AR sizes, and are connected to different large-scale patterns (Inda-Díaz et al., 2021; Prince et al., 2021; Zhou & Kim, 2019). Therefore, it is important to extend the discussion of AR flavors to the perspective of AR lifecycles and investigate whether the dominance of wind or moisture is constant throughout the lifecycle. Moreover, as the dominant mode of tropical variability on the interannual scale, ENSO is driven by a complex interaction between ocean and atmospheric circulations (Jin et al., 2006). It remains unclear whether ARs would respond differently to ENSO based on flavors. Utilizing an AR lifecycle tracking algorithm (Zhou et al., 2018), we can identify AR lifecycles and categorize the winter North Pacific AR lifecycles into two flavors: wind-dominated and moisture-dominated. The categorization method for AR flavors is different from Gonzales et al. (2020), whereas in this paper we will group ARs based on the whole lifecycle (more details later). Here, we would like to address the following questions: (a) what are the differences in the frequency, lifecycle characteristics (e.g., intensity, precipitation, and duration), and variability between wind-dominated ARs and moisture-dominated ARs? (b) how do the two AR flavors respond to climate variability (such as ENSO)?

21698996, 2022, 23, Downloaded from https://agupubs.onlinelibrary.wiley.com/doi/10.1029/2022JD037105, Wiley Online Library on [06/06/2023]. See the Terms and Conditions (https://onlinelibrary.wiley.com/terms-and-conditions) on Wiley Online Library for rules of use; OA articles are governed by the applicable Creative Commons License

21698996, 2022, 23, Downloaded from https://agupubs.onlinelibrary.wiley.com/doi/10.1029/2022JD037105, Wiley Online Library on [06/06/2023]. See the Terms and Conditions (https://onlinelibrary.wiley.com/terms-and-conditions) on Wiley Online Library for rules of use; OA articles are governed by the applicable Creative Commons License

This paper is organized as follows. In Section 2, we introduce the data and methodology for AR detection and tracking. In Section 3, we investigate the differences between the two AR flavors including climatology, lifecycle development, landfall impacts, and response to ENSO. In Section 4, we discuss the uncertainty induced by AR detection algorithms (ARDTs). Summary and discussion are provided in Section 5.

2. Data and Methods

2.1. Data

The data set used in this study is retrieved from the fifth generation of the European Centre for Medium-Range Weather Forecasts Interim Reanalysis (ERA5; Hersbach et al., 2020). We use the hourly IVT in 0.25° latitude by 0.25° longitude grids for AR detection. Hourly IWV and 850 hPa horizontal wind from ERA5 are adopted to categorize AR flavors. ERA5 hourly precipitation is used to understand AR landfall impacts. The focused period is December to February from 1979 to 2018, which is the active season for North Pacific ARs to make landfall over the U.S. West Coast (Mundhenk et al., 2016).

We investigate the connections between ARs and low-frequency climate variability such as ENSO. To identify El Niño and La Niñ events, we include the ENSO Longitude Index (ELI; Williams & Patricola, 2018), which is a metric, based on the weak-temperature gradient approximation, that captures how the average longitude of the Pacific tropical deep convection responds to changes in tropical sea surface temperature (SST) patterns. The ELI can characterize the diversity of ENSO events in a single index, it is also shown to better describe the seasonal variations in western U.S. winter precipitation compared with other ENSO indices (Patricola et al., 2020). Following Patricola et al. (2020), we define ENSO events using the December-February average of ELI: eastern Pacific El Niño (EPEN) when ELI $\geq 170°$, central Pacific El Niño (CPEN) when $170° > \text{ELI} \geq 162°$, and La Niña (NINA) when $162° > \text{ELI} \geq 152°$.

2.2. AR Detection and Tracking

We applied the Toolkit for Extreme Climate Analysis Bayesian AR Detector (TECA; O'Brien, Payne, et al., 2020; O'Brien, Risser, et al., 2020) to detect binary masks of ARs from the IVT field. The TECA-BARD includes a set of "plausible" AR detectors sampled by a Bayesian framework, which can produce AR masks similar to ARs manually identified by experts. Previous studies have shown uncertainty in the detection of ARs, due to different algorithm choices (e.g., the use of relative vs. absolute thresholds), can affect conclusions in AR analyses (Lora et al., 2020; O'Brien, Payne, et al., 2020; O'Brien, Risser, et al., 2020; Shields et al., 2018; Zhou et al., 2021). Among all global AR detections, TECA is considered more restrictive compared to others because TECA tends to capture areas close to AR cores and is one of the algorithms that detect the fewest instantaneous AR mask counts globally (Zhou et al., 2021). To explore the impact of detection uncertainty on the determination of AR flavors, we repeat the analyses in this paper with ARs detected by the algorithm developed by Guan and Waliser (2015) (GW15). The GW15 uses a relative IVT threshold along with criteria on geometric shape and direction, which is shown to be less restrictive than other ARDTs (Rutz et al., 2019; Shields et al., 2018). Our previous study shows that on average, GW15 detects twice as much as AR binary masks as TECA in a time step. We use the AR tracking algorithm developed by Zhou et al. (2018) and Zhou and Kim (2019) to identify the lifecycle of ARs based on instantaneous AR binary masks. The Zhou et al. (2018) tracking algorithm has been applied to most of the global ARDTs in the Atmospheric River Tracking Method Intercomparison Project (Zhou et al., 2021).

3. Windy ARs Versus Wet ARs

3.1. Climatology

We use the 850 hPa wind speed (UV850) and IWV to represent the dynamic and thermodynamic components of ARs. UV850 provides a representative measure of the AR winds because 850 hPa is approximately the core level where the low-level jet is typically located (Cordeira et al., 2013; Ralph et al., 2004). For each AR event, we first calculate the area-weighted averaging of UV850, IWV, and IVT at each time step along the lifecycle, and then calculate the mean of all time steps (Figure 1). Figure 1a shows that lifecycle-averaged UV850 and IWV are significantly negatively correlated: a correlation coefficient of −0.54 and a p-value of 3.62e−75. A previous study regarding midlatitude cyclones also showed that the wind speed and moisture in cyclones are negatively

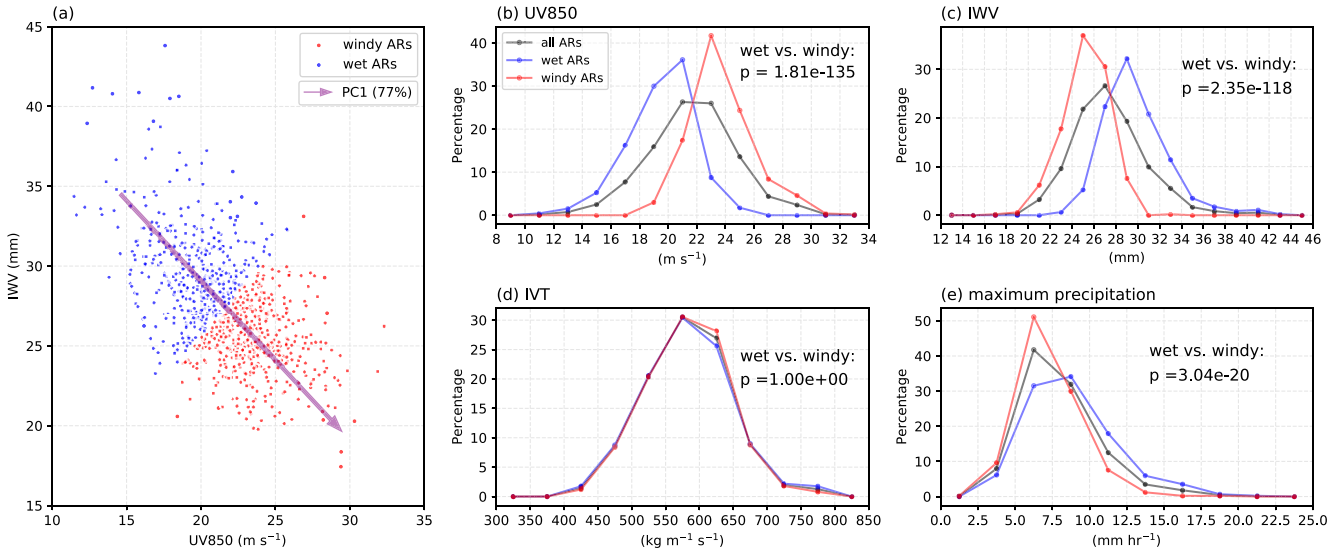

Figure 1. (a) Scatter plot of wintertime North Pacific atmospheric rivers (ARs) with the *x*-axis representing the 850 hPa wind speed (UV850), and the *y*-axis representing integrated water vapor (IWV). The purple arrow marks the direction of the first principal component. (b–e) Distribution of all ARs (black line), wet ARs (blue line), and windy ARs (red line) in (b) UV850, (c) IWV, (d) integrated vapor transport (IVT), and (e) maximum precipitation. The texts in panels (b–e) show the *p*-values of a two-tailed *t*-test between windy ARs and wet ARs.

related because the air-ocean system tends to locate stronger storms (i.e., storms with stronger wind) poleward (because moisture generally decreases in poleward direction) (Field & Wood, 2007). The categorization of AR flavors proceeds as follows. First, we perform principal component analysis (PCA) on the combined matrix of normalized UV850 and IWV associated with ARs. The first principal component (PC1) explains 77% of the variance. Next, we project each AR lifecycle onto PC1 and categorize the ARs into two flavors based on their loading values: moisture-dominated ARs (hereafter, wet ARs) and wind-dominated ARs (hereafter, windy ARs) (Figure 1a). There are 745 events marked as wet ARs and 838 events for windy ARs over 39 winters. One major difference in the determination of AR flavors between this study and Gonzales et al. (2020) is that the seasonal change of the mean states (such as the seasonal shift of jet stream and moisture background) is considered here, where they are removed in Gonzales et al. (2020). We intend to keep the background states because past studies showed that the propagation of ARs is largely impacted by the background circulation (Guirguis et al., 2019; Zhou & Kim, 2019). Although disagreements may occur between our method and Gonzales et al. (2020) due to different choices of ARDTs and different focus of scientific questions (Gonzales et al. (2020) focus on landfalling ARs only), we speculate consensuses exist in the categorization of AR flavors. For example, the wet ARs with extra strong moisture here (e.g., top left corner of Figure 1a) are most likely marked as wet ARs as well in Gonzales et al. (2020). However, addressing the agreements and disagreements between the two methods requires a further detailed comparison and is beyond the scope of the current study.

The distribution of UV850 and IWV are significantly different between windy ARs and wet ARs (Figures 1b and 1c). The mean UV850 of windy ARs (27.3 m/s) is 21% stronger compared with that of wet ARs (22.5 m/s). Contrarily, the mean IWV of wet ARs is about 30.4 mm, which is 17% higher than that of windy ARs (24.9 mm). Interestingly, with such distinct distribution in wind and moisture, the IVT distribution is almost identical for the two AR flavors (Figure 1d). The maximum precipitation of an AR event is calculated as the average of the maximum precipitation (within an AR binary mask) along the lifecycle. The distribution of maximum precipitation is significantly different between windy ARs and wet ARs. Wet ARs are more likely to have intense precipitation (Figure 1e). When forecasting AR-related precipitation, one of the most common assessments in past studies is the magnitude of IVT (Ralph et al., 2019), given that precipitation and IVT have been shown to be strongly correlated (Neiman et al., 2002). Figure 1 suggests that two AR events with similar IVTs could have different wind and moisture profiles, and therefore lead to different precipitation amounts. Consistent results can be found in Gonzales et al. (2020). Additionally, we examine the second mode of the PCA (Figure S1 in Supporting Information S1), which further classifies ARs into subcategories as windy ARs with stronger or weaker moisture, and wet ARs with stronger or weaker winds. Results indicate that for both windy and wet ARs, ARs with stronger

21698996, 2022, 23, Downloaded from https://agupubs.onlinelibrary.wiley.com/doi/10.1029/2022JD037105, Wiley Online Library on [06/06/2023]. See the Terms and Conditions (https://onlinelibrary.wiley.com/terms-and-conditions) on Wiley Online Library for rules of use; OA articles are governed by the applicable Creative Commons License

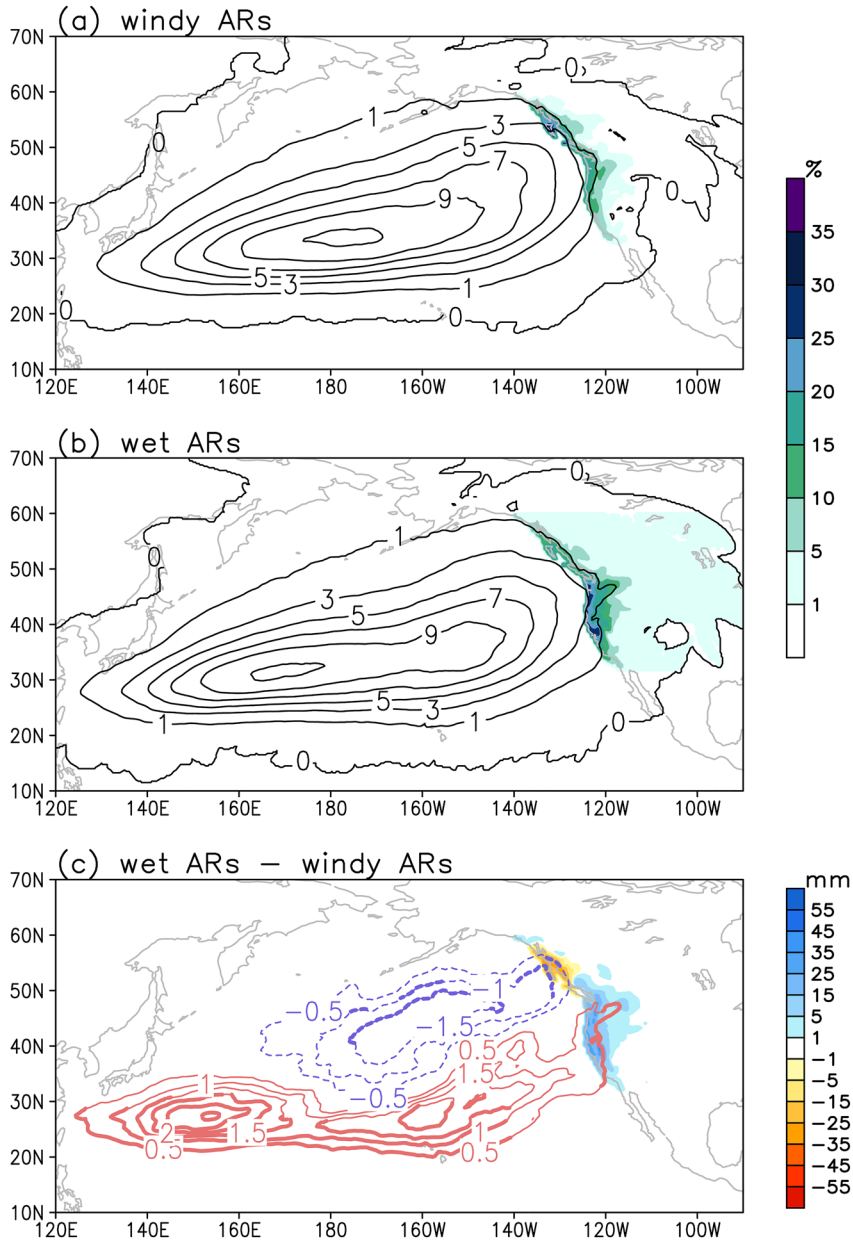

Figure 2. (a and b) Winter climatological atmospheric river (AR) frequency (contour, unit: percent of time steps) and the ratio of (a) windy AR- and (b) wet AR-associated precipitation (shading, unit: %) to total winter precipitation. (c) The difference in AR frequency (contour, unit: percent of time steps) and winter precipitation (shading, unit: mm per winter) between panels (a) and (b). The thickened contours mark the values with a *p*-value <0.05.

moisture have significantly stronger IVTs, suggesting that the IVT magnitude is mainly determined by the moisture content (Figure S1c in Supporting Information S1).

Windy ARs and wet ARs differ in terms of their climatological frequencies, associated precipitation, and inland penetration (Figure 2). Note that in Figure 2, the overland impacts (shading) are only from landfalling ARs, which are a subset of North Pacific ARs (shown in contours). Although the frequencies of both AR flavors spread across the North Pacific basin, the locations of maximum frequency differ. The maximum frequency center of windy ARs is located over the central Pacific between 30°–35°N and 170°E−170°W, while the highest frequency of wet ARs displaces westward around 30°N, 160°E−180°. By taking the difference in frequencies between the two AR flavors, we show that more wet ARs tend to occur over the subtropics between 25° and 35°N, and windy ARs

21698996, 2022, 23, Downloaded from https://agupubs.onlinelibrary.wiley.com/doi/10.1029/2022JD037105, Wiley Online Library on [06/06/2023]. See the Terms and Conditions (https://onlinelibrary.wiley.com/terms-and-conditions) on Wiley Online Library for rules of use; OA articles are governed by the applicable Creative Commons License

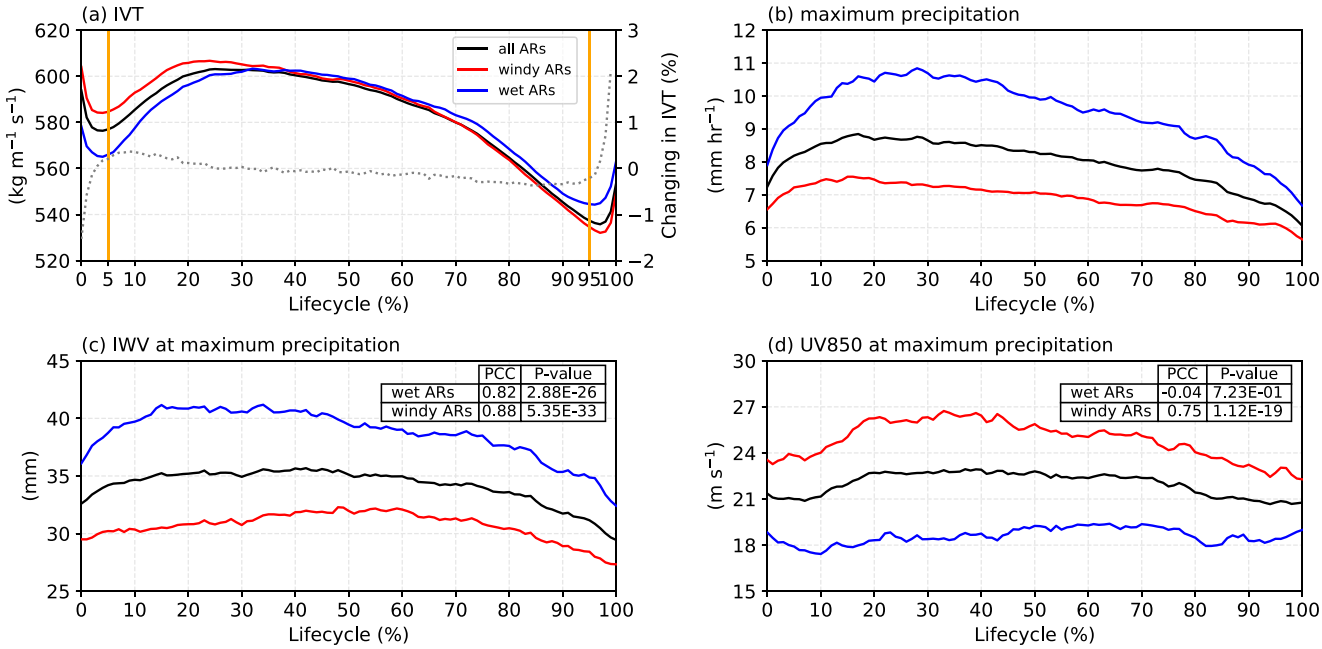

Figure 3. (a) The change in area-weighted integrated vapor transport (IVT) along atmospheric river (AR) lifecycle for all ARs (solid black line), windy ARs (red line), and wet ARs (blue line). Panels (b–d) same as panel (a), but for (b) maximum precipitation, and (c) integrated water vapor (IWV) and (d) 850 hPa wind speed (UV850) at the location of maximum precipitation. The black dotted line in panel (a) shows the relative change in IVT from the previous timestep, and the orange lines in panel (a) mark the points of 5% and 95% of the lifecycle. The table in panels (c and d) shows the Pearson correlation coefficient (PCC) and *p*-value between (c) IWV and maximum precipitation, and (d) UV850 and maximum precipitation, on windy ARs and wet ARs. The *p*-value is measured by a two-tail *t*-test.

are more frequent over the mid-latitude (Figure 2c). This is likely due to the background of poleward decreasing water vapor and stronger eastward wind in the mid-latitudes. Over the subtropics, there are two positive anomalous centers for wet ARs: one is over the western Pacific, which may be associated with tropical cyclone activities (Cordeira et al., 2013); the other one is over the eastern Pacific, which represents the well-known "Pineapple Express." Previous studies demonstrated that even with a few events, ARs that can penetrate inland are of great importance to local hydroclimate (Neiman et al., 2013; Rutz et al., 2014). Our results agree with previous literature: ARs account for up to 30% of total winter precipitation over the interior western US, even though inland-penetrating ARs only occur about 1%–3% of the total winter steps (Figures 2a and 2b). Wet ARs are more likely to penetrate further inland compared with the windy ones, possibly due to the high moisture content which can compensate for the moisture depletion when passing the topographical barriers and extend the duration of landfall. The distribution of AR-related precipitation is different between AR flavors. The wet ARs account for up to ~35% of total winter precipitation over the interior western US, especially over Oregon, Washington, and northern California (Figure 2b). The windy ARs contribute about up to 30% of total winter precipitation over British Columbia, and the contribution decreases southward. Compared with windy ARs, precipitation caused by wet ARs is about 20 mm more over the U.S. West Coast and about 5 mm more over inland regions in every winter (Figure 2c). Over British Columbia, windy ARs bring more coastal precipitation than wet ARs by an average of 25 mm per winter. More discussion of AR-related precipitation over land is provided in Section 3.3.

3.2. Lifecycle Development

It is unclear how the wind and moisture properties of ARs may change along their lifecycle. For example, will an AR event that starts as "wet" later become "windy" as it propagates? To demonstrate how the meteorological elements (wind, moisture, and precipitation) change along AR lifecycles with different lifetimes, we interpolated the AR lifecycles into 100 portions so that 0% of the lifecycle means genesis and 100% represents termination. The dashed line in Figure 3a denotes the rate of change in area-weighted AR IVT magnitude during the lifecycle. The rapid change of IVT occurs in the first and last 5% of the AR lifecycles, mostly due to the expansion or reduction of AR sizes (Figure S2 in Supporting Information S1). The first 5% of the lifecycle is generally the genesis stage, where AR starts to expand quickly to 40% more than its very first size. The expansion of AR size lowers the

21698996, 2022, 23, Downloaded from https://agupubs.onlinelibrary.wiley.com/doi/10.1029/2022JD037105, Wiley Online Library on [06/06/2023]. See the Terms and Conditions (https://onlinelibrary.wiley.com/terms-and-conditions) on Wiley Online Library for rules of use; OA articles are governed by the applicable Creative Commons License

21698996, 2022, 23, Downloaded from https://agupubs.onlinelibrary.wiley.com/doi/10.1029/2022JD037105, Wiley Online Library on [06/06/2023]. See the Terms and Conditions (https://onlinelibrary.wiley.com/terms-and-conditions) on Wiley Online Library for rules of use; OA articles are governed by the applicable Creative Commons License

magnitude of area-averaged IVT (Figure 3a). A previous study showed the expansion of size may be related to the development of low-level jet that is associated with cold fronts or cyclones (Cordeira et al., 2013). Another rapid change occurs at 95%–100% of the lifecycle when the AR size diminishes to about 40% due to moisture loss from precipitation and results in a rapid increase in the area-averaged IVT. Based on the change rate of IVT, we divide the AR lifecycles into three stages: genesis (0%–5%), mature (5%–95%), and decay (95%–100%).

Along the AR lifecycles, we record the maximum precipitation within an AR mask (MaxPrecip) to estimate the rainfall intensity associated with AR. We do not use the area-averaged precipitation because not all grid cells in an AR mask will precipitate because precipitation usually requires lifting. The MaxPrecip of each AR event is then interpolated into 100 lifecycle stages (Figure 3b). In general, the MaxPrecip of ARs increases at the first 30% of the lifecycle and gradually decreases until termination. The MaxPrecip of wet ARs is stronger than windy ARs in a range of 20%–48% during the entire lifecycle. For wet ARs, the MaxPrecip is about 8–10 mm per hour at the genesis stage and intensified by ∼37% to 10.5 mm per hour at the mature stage. The windy ARs, on the other hand, have only a 15% increase in MaxPrecip compared with their genesis. Previous studies have demonstrated that the cyclone precipitation intensity is proportional to the product of near-surface wind speed and column moisture (Pfahl & Sprenger, 2016; Yettella & Kay, 2016). Here, to estimate the relative importance of wind and moisture to AR precipitation, we record the IWV and UV850 at the point of MaxPrecip (marked as IWV_MaxP and UV850_MaxP) (Figures 3c and 3d). Figures 3b and 3c suggest that on average, wet ARs have more moisture and weaker wind compared to windy ARs through the lifecycle. As discussed in Cordeira et al. (2013) on the evolution of two AR events, even though precipitation occurs during the whole lifecycle, the IWV within an AR is supplemented by the IWV from the extratropics and subtropics via frontogenesis or IVT convergence. The IWV_MaxP of wet ARs is, on average, 26% stronger than windy ARs, which indicates that wet ARs have more IWV to support precipitation. The connection of MaxPrecip to wind or moisture is measured by the Pearson correlation coefficients (PCC; see tables in Figures 3c and 3d). For windy ARs, the PCC of IWV_MaxP and UV850_MaxP to MaxPrecip is 0.88 and 0.75, respectively. This indicates that moisture and wind are comparably important in affecting the precipitation intensity for windy ARs. However, for wet ARs, the PCC is 0.82 for IWV_MaxP and −0.04 for UV850_MaxP, suggesting that the precipitation intensity is dominated solely by moisture amount in the wet ARs. Interestingly, the majority of AR events with strong precipitation (MaxPrecip >10 mm per hour) are wet ARs with relatively weak wind (see Figure S1 in Supporting Information S1).

Previous studies have explored the relationship between ARs and extratropical cyclones. Zhang et al. (2019) show that surface pressure gradient is key for maintaining the moisture transport in ARs. A similar conclusion is drawn by Guo et al. (2020), who also highlight that the anticyclone, which is at the downstream equatorward side of the cyclone, is important for AR occurrence. To examine how windy ARs and wet ARs respond to the pressure environment, we connect ARs with their nearest sea-level pressure (SLP) minimum. Zhang et al. (2019) show that the AR IVT maximum points are mostly located over the south-southeast of the extratropical cyclones within the range of 2,500 km. Here, we find the AR-associated SLP minimum within a 2,500 km × 2,500 km box centered at the AR IVT maximum. Zhang et al. (2019) categorizes the extratropical cyclone strength into five categories: >1,010, 1,010–998, 998–986, 986–974, and <974 hPa. We group the windy ARs and wet ARs by the lifecycle-averaged SLP minimum following Zhang et al.'s (2019) categorization (Figure 4). We observe that windy ARs are connected to deeper surface pressure lows than wet ARs, which implies that windy ARs are more linked to strong extratropical cyclones, whose stronger pressure gradient supports the enhancement of low-level wind. Although most of the wet ARs are connected to pressure lows with moderate strength, they produce more precipitation than windy ARs (Figure 4b). The accumulated AR precipitation shown in (Figure 4b) is calculated by the lifecycle-accumulation of the summation of the precipitation within each AR mask along the lifecycle. For SLP minimum between 1,010 and 986 hPa, the accumulated AR precipitation by wet ARs is 25%–35% more than windy ARs. For stronger cyclones (<986 hPa), wet ARs produce 50%–80% more accumulated AR precipitation than windy ARs, which could possibly be attributed to larger precipitation area, longer lifetime, and/or higher precipitation rate. Results indicate that generally with stronger cyclones, ARs have a larger size and longer lifetime (Figure S3 in Supporting Information S1). The wet ARs, on average, last longer with a larger size than windy ARs in every cyclone intensity category (Figures S3c and S3d in Supporting Information S1). We also calculated the lifecycle average of AR precipitation averaged over AR grids with non-zero precipitation (Figure S3b in Supporting Information S1). This variable can represent the overall precipitation rate within AR during its lifecycle. The overall precipitation rate does not change much (within a change of about 10%) between cyclone intensities. Interestingly, windy ARs have a slightly higher precipitation rate in stronger cyclones (<998 hPa).

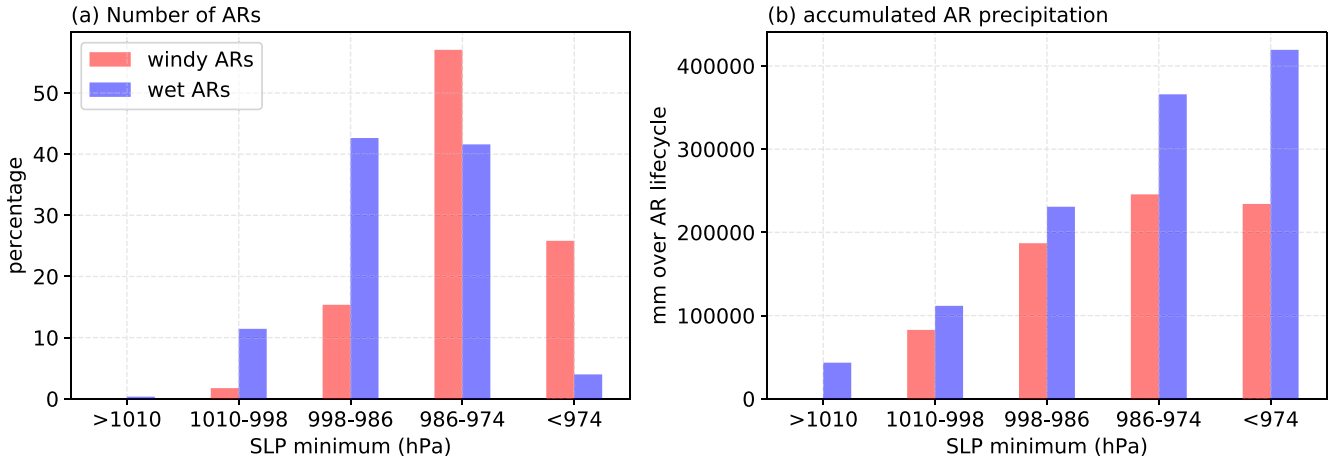

Figure 4. (a) The number of atmospheric river (AR) by different groups of minimum sea-level pressure (SLP, unit: hPa) in percentage. Panel (b) same as panel (a), but for accumulated AR precipitation over the lifecycle (unit: mm).

Therefore, the greater accumulated precipitation of wet ARs is mainly due to their larger coverage (size) and longer duration (lifetime).

3.3. Landfalling Impacts

To better address the hydrological impacts when an AR makes landfall over North America, the landfalling ARs are categorized into five scales based on the maximum IVT magnitude at landfall and landfall duration (details in Ralph et al. (2019)). The AR scales assess the level of beneficial and hazardous impacts of landfalling ARs. For western North America, the Cat 1 and Cat 2 ARs are most beneficial with little hazardous impacts, Cat 3 ARs contain a balance of beneficial and hazardous, and Cat 4 and Cat 5 ARs are most hazardous. The Ralph et al. (2019) AR scales are grid-point-based, meaning that for the same landfalling AR event, AR scales vary in different locations. In this study, it is more convenient to label each landfalling AR with only one AR category. Instead of using the grid-point-based maximum IVT and landfall duration (Ralph et al., 2019), here, the landfalling ARs are categorized using the maximum IVT over land during the entire landfall and the landfall duration of the whole event, which is the same method as our previous work (Zhou et al., 2021). Therefore, the AR categories in this study potentially overestimate the events. On average, about 10 ARs make landfall over North America every winter.

We estimate the AR-related precipitation (hereafter, AR precipitation) by calculating the precipitation within the binary AR masks. On average, ARs account for 40%–50% of total winter precipitation along the coast of British Columbia, and the AR contribution decreases southward, with about 40% over Washington and Oregon, and 25%–40% over California (Figures 2a and 2b). Our results are within the range of previous studies that showed the contribution of AR precipitation to the total precipitation. Large uncertainty exists in the estimation of AR's contribution to total precipitation, which can range from 20% to 70%, depending on different studies using different detection methods and reanalyses of various horizontal resolutions (Dettinger et al., 2011; Gershunov et al., 2017; Lavers & Villarini, 2015; Shields et al., 2018). Besides that different ARDT can induce uncertainty in AR precipitation (Leung et al., 2022), one source of the large uncertainty is that a higher temporal resolution can increase the percentage of AR precipitation because the duration of an AR is measured in finer time steps (Collow et al., 2022). Precipitation data sources could also contribute to the difference in AR precipitation. For example, with hourly ERA5 reanalysis, ARs detected by Guan and Waliser (2015) contribute 60%–80% of total winter precipitation over North America (summing the left column of Figure 9). However, the contribution drops to 30% when using daily Global Precipitation Climatology Project product (Figure 2c in Shields et al. (2018)). Other studies highlighted that precipitation reanalyses are biased high compared to satellite products and that the consensus between reanalyses and satellite products are regional dependent (Arabzadeh et al., 2020; Collow et al., 2022). It is also important to note that different reanalysis products produce different results for AR climatology, which is also shown in Collow et al. (2022).

21698996, 2022, 23, Downloaded from https://agupubs.onlinelibrary.wiley.com/doi/10.1029/2022JD037105, Wiley Online Library on [06/06/2023]. See the Terms and Conditions (https://onlinelibrary.wiley.com/terms-and-conditions) on Wiley Online Library for rules of use; OA articles are governed by the applicable Creative Commons License

21698996, 2022, 23, Downloaded from https://agupubs.onlinelibrary.wiley.com/doi/10.1029/2022JD037105, Wiley Online Library on [06/06/2023]. See the Terms and Conditions (https://onlinelibrary.wiley.com/terms-and-conditions) on Wiley Online Library for rules of use; OA articles are governed by the applicable Creative Commons License

We break down AR's contribution to total winter precipitation by AR categories. The AR's contribution to total winter precipitation increases with the AR category (Figures 5a–5e). For Cat 1 and 2 ARs, the maximum contribution is between 40° and 60°N, where Cat 1 and 2 ARs only contributes about 2%–4% to total winter precipitation (Figures 5a and 5b). The maximum contribution shifts southward from Cat 3 to Cat 5 ARs (Figures 5c–5e). For Cat 4 and 5 ARs, the maximum contribution is over Oregon, Washington, the northern California, with about 10%–12% contribution, respectively. The higher contributions of Cat 4 and 5 ARs over the northern part of the U.S. West Coast, especially between 40° and 50°N, are consistent with Ralph et al. (2019).

It is of interest to compare how windy ARs and wet ARs are categorized by the AR scale since the two AR flavors have similar distributions of IVT magnitude (Figure 1d), which is one of the main metrics used in the AR scale. We calculated the number of landfalling ARs by counting ARs hitting western North America between 32° and 60°N. Since the AR precipitation is associated with both precipitation frequency and intensity, we also calculated the precipitation intensity by dividing the AR precipitation by AR frequency. Figure S4 in Supporting Information S1 shows the zonal average (5° box along the west coast) of coastal AR precipitation, AR frequency, and AR precipitation intensity. For Cat 1 and 3, the number of windy ARs is comparable with wet ARs, with only 1%–3% more than the latter (Figure 6). Although the number of Cat 2 windy ARs is approximately 50% more than that of Cat2 wet ARs, the difference in spatial distribution between wet and windy Cat 2 AR precipitation is consistent with Cat 1 and 3: more windy AR frequencies appear between 40° and 60°N and therefore windy ARs are more associated with precipitation over British Columbia (Figures 5f–5h). Wet ARs, on the other hand, contribute more precipitation to the U.S. West Coast. More Cat 4 ARs are marked as wet ARs instead of windy ARs. The difference decreases for Cat 5 ARs where wet ARs are only slightly over windy ARs (Figure 6). However, for spatial distribution, more wet AR frequency occurs almost over the entire U.S. West Coast, which results in more wet AR precipitation compared to windy ARs (Figures 5i and 5j). We found that the difference in AR precipitation between AR flavors is mainly attributed to differences in AR frequency (Figure S4 in Supporting Information S1). Therefore, the spatial difference between Cat 4 and 5 AR flavors is likely due to wet ARs having wider landfall coverage and longer duration than windy ARs, even though the two AR flavors have comparable counts. A previous study by Gonzales et al. (2020) on AR flavors has shown that windy landfalling ARs have a higher daily precipitation rate over U.S. West Coast. Here, we show that AR precipitation over U.S. West Coast is mostly contributed by wet ARs. Although our results may seem contradictory to Gonzales et al. (2020), the two studies are not calculating the same variables, where we use the winter-accumulated precipitation and they calculated the daily precipitation rate. The latitudinal variation of precipitation intensity indicates that in some categories (e.g., Cat 1 and 2), windy ARs have higher precipitation intensity over the U.S. West Coast, especially over California (Figure S4 in Supporting Information S1), which is consistent with Gonzales et al. (2020).

3.4. Connections to ENSO

Numerous studies have examined how North Pacific ARs respond to ENSO (Guan & Waliser, 2015; H. Kim et al., 2017; Mundhenk et al., 2016; Payne & Magnusdottir, 2014; Ryoo et al., 2013). Generally, during EPEN winters (i.e., cold Tongue El Niño, hereafter EPEN), with the anomalously warm SST over the eastern Pacific, the Aleutian Low is deepened which induces an anomalous cyclonic flow over the northeastern Pacific (gray contours in Figure 7d). Note that the circulation and SST anomalies shown in the second and third rows of Figure 7 (contours) are based on all winter days under the specified ENSO conditions. Associated with the eastward extended subtropical jet (magenta contours in Figure 7d), AR activity is increased in the subtropics between 25°N and 35°N across the Pacific basin (Figure 7a). For CPEN winters (i.e., Warm Pool El Niño, hereafter CPEN), the anomalously warm SST center is located over the center of the equatorial Pacific. The corresponding teleconnection patterns have weaker amplitude compared with EPEN (Figure 7e). The frequent landfall locations of ARs over the U.S. West Coast shift southward in CPEN compared with EPEN (Figures 7a and 7b), which can bring more rainfall to southern California (H. Kim et al., 2017). For NINA winters, with cold SST anomalies concentrated over the eastern Pacific, the Aleutian Low is weakened as a high-pressure anomaly appears over the northeastern Pacific (Figure 7f). The subtropical jet is retracted westward. Driven by the anomalous circulation, more ARs occur at higher latitudes between 40° and 60°N, and fewer ARs appear between 25° and 40°N over the northeastern Pacific (Figure 7c).

The different flavors have distinctly different responses to changes in ENSO (the second and third rows of Figure 7). Note that the summation of the anomalous windy and wet AR frequencies (the second and third rows

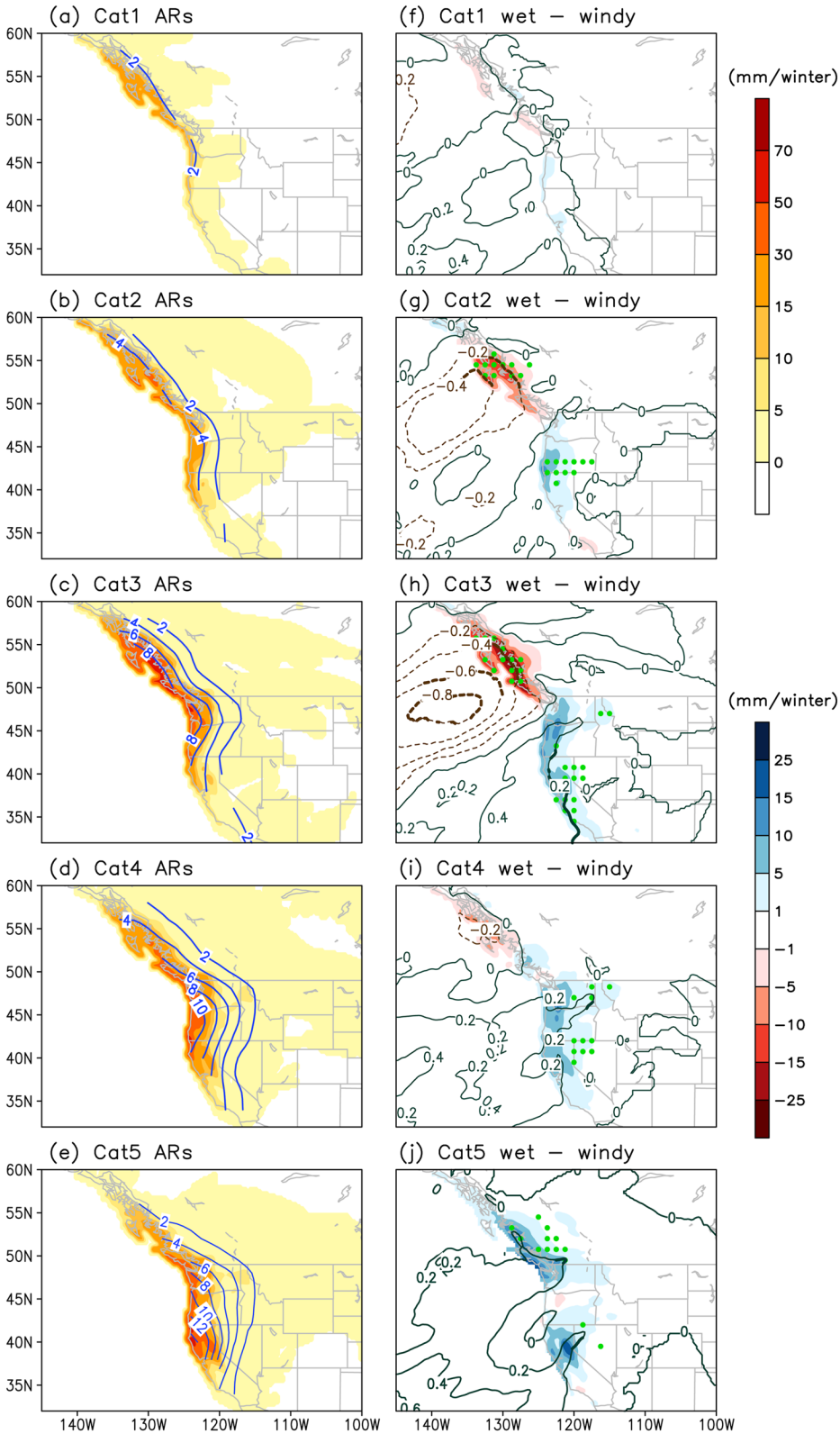

Figure 5.

21698996, 2022, 23, Downloaded from https://agupubs.onlinelibrary.wiley.com/doi/10.1029/2022JD037105, Wiley Online Library on [06/06/2023]. See the Terms and Conditions (https://onlinelibrary.wiley.com/terms-and-conditions) on Wiley Online Library for rules of use; OA articles are governed by the applicable Creative Commons License

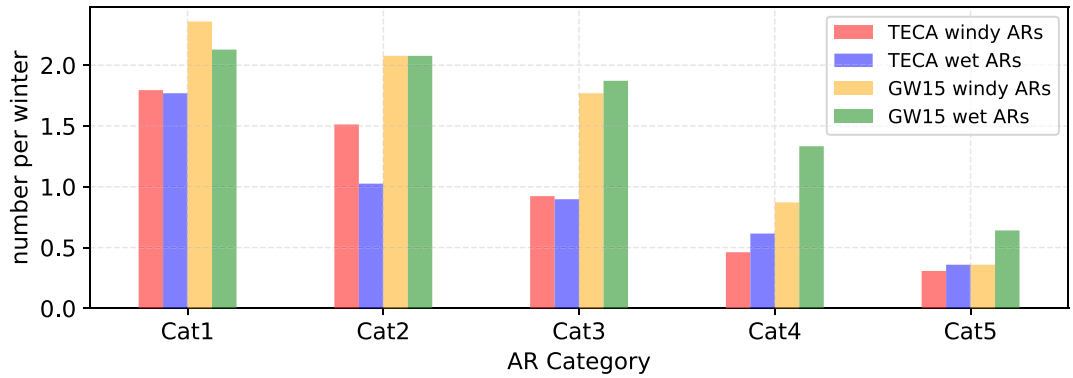

Figure 6. The number of landfalling atmospheric rivers (ARs) per winter over western North America (between 32° and 60°N) from five categories detected by Toolkit for Extreme Climate Analysis (TECA) (red and blue bars; O'Brien, Payne, et al., 2020; O'Brien, Risser, et al., 2020) and GW15 (yellow and green bars; Guan & Waliser, 2015).

of Figure 7) equals the total anomalous AR frequency (the top row of Figure 7). The changes of windy ARs are associated with the circulation pattern. During EPEN, the windy AR frequency is significantly increased in the subtropics, especially at the south branch of the anomalous low (Figure 7d). Similar changes in windy AR frequency occur in CPEN but with weaker amplitude (Figure 7e). During NINA, a zonal band of decreased windy AR frequency occurs in the subtropics, which is associated with the anomalous high (Figure 7f). Unlike the windy ARs that are modulated by ENSO teleconnections, the wet ARs are largely affected by the local change of SST (Figures 7g–7i). During EPEN, the wet AR frequency is significantly increased over the northwestern Pacific because more moisture is evaporated in the atmosphere due to the local warm SST anomaly. The negative anomaly of wet AR frequency appears over the central Pacific between 20° and 50°N, which overlaps with the cold SST anomaly below (Figure 7g). During CPEN winters, cold SST anomalies spread over most of the North Pacific basin, which leads to a decrease in wet AR activity (Figure 7h). During NINA, warm SST anomalies fill the western and central northern Pacific with a maximum of around 35°N and 160°W. Consequently, the wet AR activity is significantly increased over these regions (Figure 7i). Closer inspection of the anomalous patterns between windy ARs and wet ARs shows that in some locations, the ENSO response is nearly opposite between AR flavors, which explains the asymmetry of total AR responses to different phases of ENSO. For example, the positive AR frequency anomalies over subtropics during El Niño are almost entirely attributed to more frequent windy ARs. Also, the positive AR anomalies over mid-latitude between 40° and 60°N during NINA are contributed by the increased wet ARs. To summarize, the ARs' responses to ENSO can be attributed to AR flavors to different extents depending on locations. The changes in windy ARs are mainly induced by the large-scale circulation pattern in response to ENSO, which are more prevalent over the subtropics. The changes of wet ARs are more prevailing over the mid-latitudes, which are associated with SST anomalies related to ENSO.

4. Uncertainty From AR Detection Algorithms

There have been extensive discussions on the uncertainty in AR measures due to ARDTs. In particular, the occurrence and areal coverage of landfalling ARs are shown to have a great range of diversity based on different ARDTs. For example, Shields et al. (2018) shows that the landfalling AR frequency over the U.S. West Coast can range from 2 counts to 65 counts in 3-hourly time steps for the month of February with various choices of ARDTs. It is also shown in Shields et al. (2018) that AR's contribution to total winter precipitation over California can vary from 30% to 50% by different ARDTs. The ARDTs can be assessed with a level of restrictiveness (Rutz et al., 2019). The TECA-BARD algorithm used in this study is considered a restrictive algorithm. This means that the detected AR masks by TECA-BARD are fewer or smaller than ARs detected by other algorithms (O'Brien, Payne, et al., 2020; O'Brien, Risser, et al., 2020). Here, to provide a comprehensive discussion on windy ARs and

Figure 5. (a–e) Winter accumulated atmospheric river (AR) precipitation (shading, mm per winter) attributed to Category 1–5 ARs. Contours: Percentage of winter-accumulated AR precipitation to the winter-accumulated total precipitation. The contours are interpolated into a 1° × 1° grid to provide a clear and smooth representation. (f–j) Difference between wet ARs and windy ARs under the same AR category on precipitation (shading, mm per winter) and AR frequency (contour, percent of time steps). The thickened contours and green dots in the second column mark the values with a p-value <0.05. For cleaner presentation, the green dots are plotted every five grids.

21698996, 2022, 23, Downloaded from https://agupubs.onlinelibrary.wiley.com/doi/10.1029/2022JD037105, Wiley Online Library on [06/06/2023]. See the Terms and Conditions (https://onlinelibrary.wiley.com/terms-and-conditions) on Wiley Online Library for rules of use; OA articles are governed by the applicable Creative Commons License

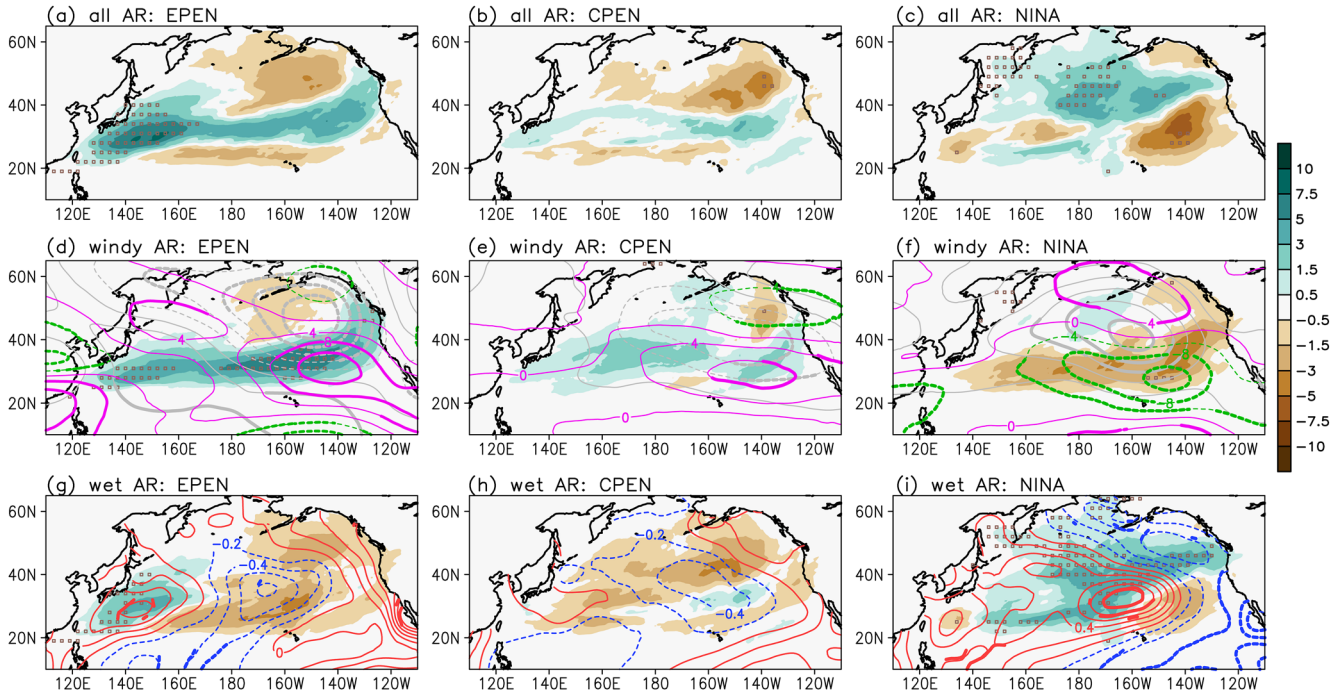

Figure 7. Composite of anomalous atmospheric river (AR) frequency (shading, unit: percent of time steps, note that the intervals are uneven) for (upper row) all winter ARs, (middle row) windy ARs, and (bottom row) wet ARs in (left column) eastern Pacific El Niño (EPEN), (middle column) central Pacific El Niño (CPEN), and (right column) eastern Pacific La Niña (NINA) winters. The gray dots denote the area with a *p*-value smaller than 0.05. Also in the middle row: winter anomalous 200 hPa zonal wind (magenta and green contours, unit: m/s) and anomalous 500 hPa geopotential height (gray contours, interval: 20 m) during all winter days under the specified El Niño Southern Oscillation (ENSO) conditions. Also in the bottom row: sea surface temperature anomaly (red and blue contours, unit: °C) under the specified ENSO conditions. All thickened contours show areas with a *p*-value smaller than 0.05.

wet ARs and to investigate the robustness of the previous results, we did the same analysis on the ARs detected by Guan and Waliser (2015) (hereafter, GW15), which is one of the less restrictive algorithms.

The distributions of AR-associated UV850 and IWV identified by GW15 are more scattered than those by TECA (Figure 8). The magnitude of GW15 UV850 ranges from 5 to 30 m s^{-1}, which is broader than TECA UV850 (10–30 m s^{-1}). An even broader range occurs in IWV in GW15, which ranges from 5 to 65 mm. The IWV range

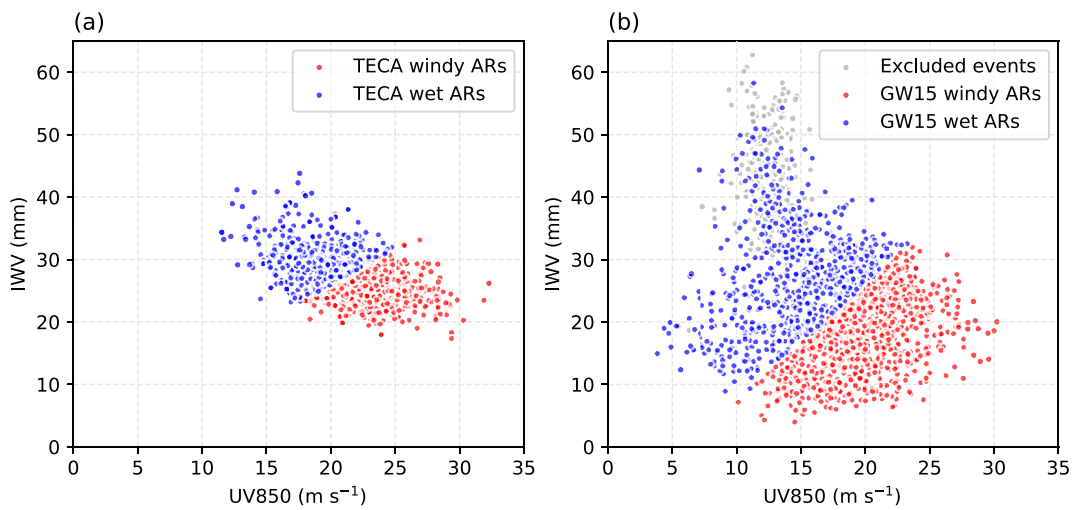

Figure 8. Scatter plot of the atmospheric river (AR)-associated 850 hPa wind speed (UV850) against integrated water transport (IWV) for ARs detected by (a) TECA-BARD and (b) GW15. Panel (a) is a replot of Figure 1a. The gray dots in panel (b) marks a subset of events excluded from the AR flavor calculation.

21698996, 2022, 23, Downloaded from https://agupubs.onlinelibrary.wiley.com/doi/10.1029/2022JD037105, Wiley Online Library on [06/06/2023]. See the Terms and Conditions (https://onlinelibrary.wiley.com/terms-and-conditions) on Wiley Online Library for rules of use; OA articles are governed by the applicable Creative Commons License

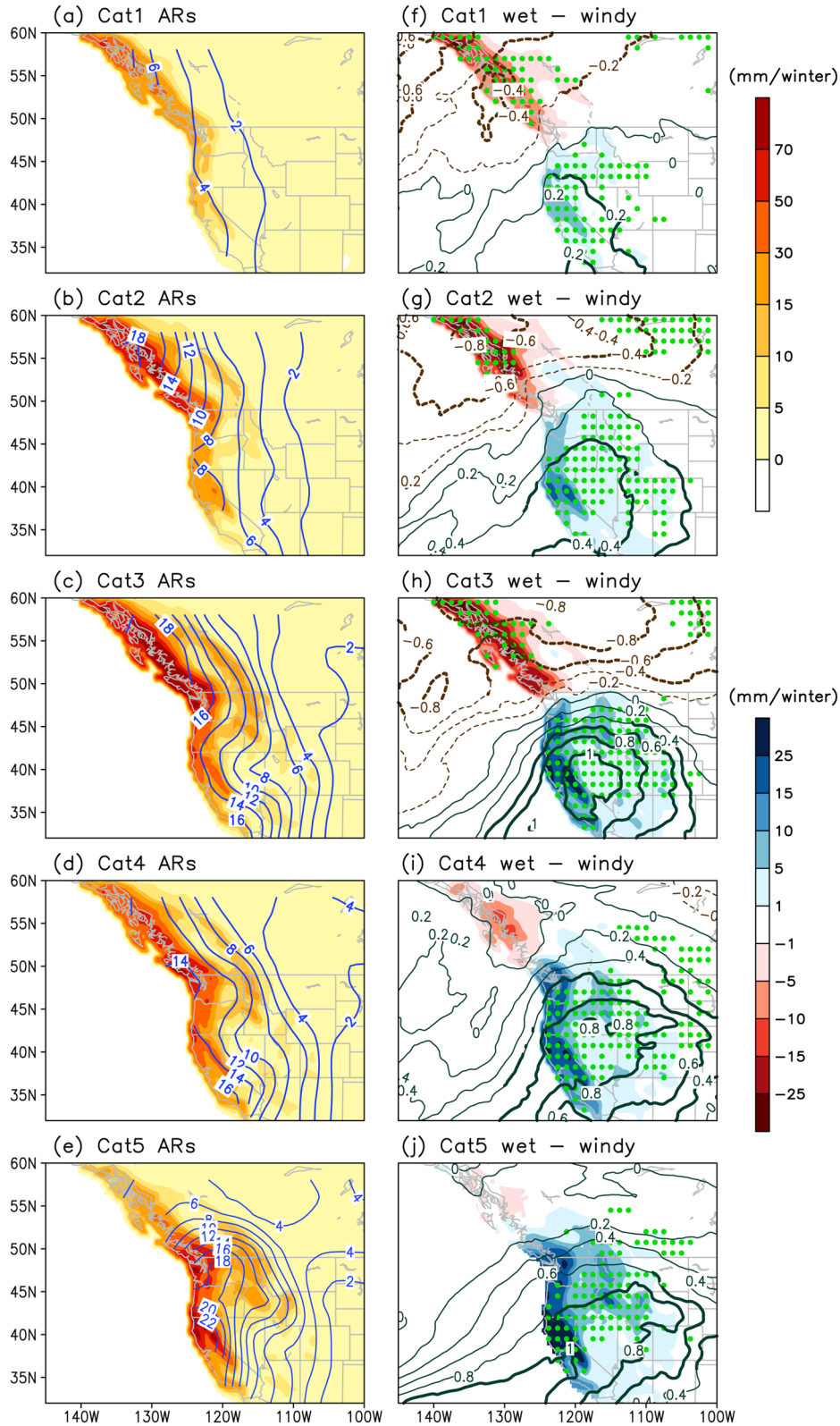

Figure 9. Same as Figure 5, but using atmospheric rivers detected by Guan and Waliser (2015).

21698996, 2022, 23, Downloaded from https://agupubs.onlinelibrary.wiley.com/doi/10.1029/2022JD037105, Wiley Online Library on [06/06/2023]. See the Terms and Conditions (https://onlinelibrary.wiley.com/terms-and-conditions) on Wiley Online Library for rules of use; OA articles are governed by the applicable Creative Commons License

21698996, 2022, 23, Downloaded from https://agupubs.onlinelibrary.wiley.com/doi/10.1029/2022JD037105, Wiley Online Library on [06/06/2023]. See the Terms and Conditions (https://onlinelibrary.wiley.com/terms-and-conditions) on Wiley Online Library for rules of use; OA articles are governed by the applicable Creative Commons License

in TECA is 15–45 mm. There is a subset (about 15% of total AR events, gray dots in the upper left of Figure 8b) of GW15-detected AR events that have different characteristics than others, which have strong IWV (30–60 mm) and moderate wind speed of 7–17 m s^{-1}. Examining further, we find that the majority of these events occur to the south of 25°N and travel within a latitude and longitude range of 10°. These events may be tropical disturbances picked up by the GW15 (Lora et al., 2020; Zhou et al., 2021). To reduce the impact of tropical disturbances, we filter out these events before the PCA process by excluding events that meet these three criteria: lifecycle-averaged latitude <25°N, the longitude and latitude difference between genesis and termination <10°. After removing the tropical disturbances, the GW15 detects approximately 5% more AR lifecycles compared to TECA. It is worth noting that the method that we used to categorize AR flavors is dependent on data sets, which means the eigenvalues and loading patterns are different between TECA and GW15. As a result, in the 39 winters, 707 events are categorized as wet ARs, and 949 events as windy ARs. The number of windy ARs is 34% more than wet ARs for GW15 detection.

Although GW15 detects more windy ARs over the northern Pacific, the number of GW15-detected landfalling windy ARs is comparable with wet ARs, which is about eight windy ARs and eight wet ARs per winter (summing all categories in Figure 6). The number of Cat 1 windy ARs is about 10% more than Cat 1 wet ARs. For Cat 2 ARs, the average numbers of the two AR flavors are the same. Wet ARs are dominant for Cat 3–5 ARs, where the number of wet ARs is 10%, 53%, and 78% more than windy ARs for Cat 3, 4, and 5, respectively. Overall, GW15 detects twice as much as the landfalling ARs detected by TECA, which is consistent with our previous study (Zhou et al., 2021). The GW15-detected AR precipitation is overall 50% more along the coast, and above 90% more inland compared to TECA-detected ARs (not shown). The AR's contribution to total winter precipitation by GW15 almost doubles the value by TECA (Figures 9a–9e). The main reason is that, despite the rapid decrease in moisture over land, GW15 captures more inland penetration by using a relative IVT threshold (Figure 9) (Zhou et al., 2021). This agrees with the results in Lora et al. (2020), where they show that GW15 has a higher frequency of "false positives" over land, which means GW15 includes more landfalling ARs than most of the other ARDTs (i.e., six or more ARDTs of total 14 ARDTs in Lora et al. (2020)). Meanwhile, Lora et al. (2020) also shows that TECA has relatively frequent "false negatives" along the west coast of North America, meaning that TECA does not detect as many landfall activities as other ARDTs. Also, due to less restrictive detection criteria, the landfall duration is potentially longer in GW15. In other words, a Cat 1 TECA-detected AR may be categorized as a Cat 2 in GW15-detected ARs because of the longer landfall duration. This is reflected in Figure 6, where the relative AR counts between GW15 and TECA are not consistent between AR categories. For example, GW15 detected 1.25 times more Cat 1 ARs and 2 times more Cat 3–4 ARs than TECA. In addition, the differences in AR precipitation between GW15-detected wet ARs and windy ARs are in good agreement with TECA, except that the AR precipitation by GW15 has greater amplitude (Figures 9f–9j).

As for the AR-ENSO connection, the total changes in AR frequency are almost dominated by windy ARs (Figures S5d–S5f in Supporting Information S1). Although in small amplitude, changes in wet ARs detected by GW15 are consistent with the local SST anomaly pattern (Figures S4g–S4i in Supporting Information S1), which agree with TECA's results. Overall, the total AR changes in GW15 agree with TECA results to some extent, except that the anomalous AR frequency in GW15 is in greater amplitude than that in TECA. GW15 also captures the AR anomalies at higher latitudes (≥60°N) (Figure S5 in Supporting Information S1).

To summarize, despite amplitude discrepancies in AR frequency and AR precipitation, the overall findings on windy AR and wet AR characteristics and the connection to ENSO are mostly consistent between TECA and GW15. Both ARDTs suggest that windy ARs are more prevalent in the lower-category ARs (e.g., Cat 1 and 2) with a higher frequency between 40° and 60°N and make more contribution to the precipitation over the British Columbia. We showed wet ARs are more prevalent in Cat 4–5, especially over the U.S. West Coast. As discussed in Rutz et al. (2019), each ARDT was developed for a different scientific question. Although robust results of AR flavors are shown between GW15 and TECA, future research related to AR flavors should choose ADRT carefully based on the focused question. For example, the GW15 would be more suitable for AR flavors in high latitudes, and TECA can benefit from questions related to the dynamic mechanisms of AR flavors.

21698996, 2022, 23, Downloaded from https://agupubs.onlinelibrary.wiley.com/doi/10.1029/2022JD037105, Wiley Online Library on [06/06/2023]. See the Terms and Conditions (https://onlinelibrary.wiley.com/terms-and-conditions) on Wiley Online Library for rules of use; OA articles are governed by the applicable Creative Commons License

5. Summary and Discussion

Our study aims to distinguish the characteristics of wind-dominated (windy) and moisture-dominated (wet) ARs given similar IVT magnitude. Focusing on the winter seasons, we apply the TECA BARD detection algorithm to identify instantaneous AR masks from ERA5 reanalysis and use the Zhou et al. (2018) tracking method to track the AR lifecycle. We classify the wintertime North Pacific ARs as windy ARs or wet ARs using the PCA analysis on AR-related wind and moisture. With a nearly identical distribution of IVT magnitude, the mean wind speed of windy ARs is 27% stronger than wet ARs, and the mean moisture is 22% weaker. The windy ARs are more active over the mid-latitudes and contribute about 25% of total winter precipitation over British Columbia. The wet ARs occur more frequently over the subtropics and contribute about 30% of winter total precipitation over California. Windy ARs are more connected to stronger surface pressure lows, whose strong pressure gradient favors the intensification of AR wind. Although most of the wet ARs are associated with surface lows with weaker intensity, wet ARs still produce more rainfall than windy ARs, due to their larger size and longer lifetime. The windy ARs and wet ARs have comparable contributions to precipitation brought by Cat 1–3 landfalling ARs and their contribution differ by locations. Wet ARs are the dominant contributor to precipitation from extreme or exceptional ARs (Cat 4 and 5), even the number of Cat 4/5 wet ARs is not significantly different from windy ARs.

We demonstrate that ENSO modulates the windy ARs and wet ARs via different processes. During El Niño, the extended subtropical jet and the deepened Aleutian Low foster a zonal band of positive anomalies of windy AR frequency that emerges over the subtropics. Meanwhile, the cold SST anomalies over the mid-latitudes lead to reduced wet AR frequency. The windy ARs have similar patterns in response to the two flavors of El Niño, despite the that the amplitude of AR anomalies is greater in EPEN than CPEN. For wet ARs, with different longitude of the tropical SST warming and mid-latitude SST cooling, the anomalous negative wet AR frequency is shifted when comparing EPEN and CPEN. During NINA winters, the occurrence of windy ARs is significantly decreased due to the retracted subtropical jet and weakened Aleutian Low. Also, enhanced wet AR activity occurs due to the warm SST anomaly. ENSO's impact on AR flavors suggests that differentiating ARs with distinct characteristics can help us to better understand their connections to modes of climate variability. Our study shows that the response of ARs to ENSO is considered as the superposition of two AR flavors, which could help to explain the variance of AR response in different ENSO cases (Patricola et al., 2020).

One source of AR uncertainty comes from detection algorithms. As discussed in Section 4, the less restrictive GW15 algorithm shows similarity in the characteristics and variability of windy ARs and wet ARs, although discrepancy exists in the amplitude of AR frequency and AR precipitation. With different algorithm designs, the boundary of AR objects varies substantially, which explains the large discrepancies in AR's impact on the land. The comparison of algorithms supports the conclusion in previous papers that algorithm recommendation is needed for specific scientific questions. While less restrictive algorithms are more recommended for impact studies (such as AR-associated heavy rain and flooding), more restrictive algorithms are suitable for addressing the physical processes associated with ARs (such as the mechanisms associated with wind-dominated and moisture-dominated ARs).

Characterizing ARs into different "flavors" has great implications for different research topics. Questions remain on why ARs can have different flavors. The difference in the connection to extratropical cyclones and associated precipitation implies that different processes may act together in the wind and moisture environment to form ARs and the dominant process may determine the AR flavors. Also, AR flavors can help to understand changes in ARs in the future climate. Past studies generally consider how changes in future dynamic and thermodynamic processes can influence AR as a whole. Here, we demonstrate that ARs with different flavors can respond to dynamic and thermodynamic forcings to different extents, which provides a way to quantify the relative contributions from these forcings. Future research will include evaluating the representation of AR flavors in climate model simulations, and understanding how different AR flavors will respond to the warming climate.

Data Availability Statement

The Guan and Waliser's (2015) AR detection code can be obtained from Guan (2021, https://doi.org/10.25346/S6/SJGRKY). The ERA5 reanalysis is downloaded from the Copernicus Climate Change Service (C3S) Climate Data Store. The results contain modified Copernicus Climate Change Service information 2020. Neither the European Commission nor ECMWF is responsible for any use that may be made of the Copernicus information

21698996, 2022, 23, Downloaded from https://agupubs.onlinelibrary.wiley.com/doi/10.1029/2022JD037105, Wiley Online Library on [06/06/2023]. See the Terms and Conditions (https://onlinelibrary.wiley.com/terms-and-conditions) on Wiley Online Library for rules of use; OA articles are governed by the applicable Creative Commons License

or data it contains. The website is https://cds.climate.copernicus.eu/cdsapp%23%21/dataset/reanalysis%2Dera5%2Dpressure%2Dlevels%3Ftab%3Dform. The Extended Reconstructed SST v5 data is provided by the NOAA/OAR/ESRL PSL, Boulder, Colorado, USA, from their website at https://psl.noaa.gov/data/gridded/data.noaa.ersst.v5.html. Documentations of TECA including installation and application examples are at https://github.com/LBL-EESA/TECA. Outputs from Zhou et al. (2018) can be obtained from Zhou et al. (2022, https://doi.org/10.5281/zenodo.6998797).

Acknowledgments

The authors would like to express our gratitude to three anonymous reviews for the time and effort spent in reviewing our manuscript and for their constructive comments which have helped us substantially improved upon the original draft. This study was funded by the U.S. Department of Energy, Office of Science, Office of Biological and Environmental Research, Regional and Global Climate Modeling Program (RGCM) under "Calibrated and Systematic Characterization, Attribution and Detection of Extremes (CASCADE)" Science Focus Area (Award DE-AC02-05CH11231) and "Cooperative Agreement to Analyze Variability, Change and Predictability in the Earth System (CATALYST)" (Award DE-SC0022070). This project was also supported by the Environmental Resilience Institute, funded by the Indiana University's Prepared for Environmental Change Grand Challenge initiative. Analysis was performed using the National Energy Research Scientific Computing Center (NERSC).

References

Arabzadeh, A., Ehsani, M. R., Guan, B., Heflin, S., & Behrangi, A. (2020). Global intercomparison of atmospheric rivers precipitation in remote sensing and reanalysis products. *Journal of Geophysical Research: Atmospheres*, *125*(21), e2020JD033021. https://doi.org/10.1029/2020JD033021

Bao, J. W., Michelson, S. A., Neiman, P. J., Ralph, F. M., & Wilczak, J. M. (2006). Interpretation of enhanced integrated water vapor bands associated with extratropical cyclones: Their formation and connection to tropical moisture. *Monthly Weather Review*, *134*(4), 1063–1080. https://doi.org/10.1175/Mwr3123.1

Collow, A. B. M., Shields, C. A., Guan, B., Kim, S., Lora, J. M., McClenny, E. E., et al. (2022). An overview of ARTMIP's tier 2 reanalysis intercomparison: Uncertainty in the detection of atmospheric rivers and their associated precipitation. *Journal of Geophysical Research: Atmospheres*, *127*(8). e2021JD036155. https://doi.org/10.1029/2021JD036155

Cordeira, J. M., Ralph, F. M., & Moore, B. J. (2013). The development and evolution of two atmospheric rivers in proximity to Western North Pacific tropical cyclones in October 2010. *Monthly Weather Review*, *141*(12), 4234–4255. https://doi.org/10.1175/Mwr-D-13-00019.1

Dacre, H. F., Clark, P. A., Martinez-Alvarado, O., Stringer, M. A., & Lavers, D. A. (2015). How do atmospheric rivers form? *Bulletin of the American Meteorological Society*, *96*(8), 1243–1255. https://doi.org/10.1175/bams-d-14-00031.1

Dettinger, M. D. (2011). Climate change, atmospheric rivers, and floods in California – A multimodel analysis of storm frequency and magnitude changes. *Journal of the American Water Resources Association*, *47*(3), 514–523. https://doi.org/10.1111/j.1752-1688.2011.00546.x

Dettinger, M. D. (2013). Atmospheric rivers as drought busters on the US West Coast. *Journal of Hydrometeorology*, *14*(6), 1721–1732. https://doi.org/10.1175/Jhm-D-13-02.1

Dettinger, M. D., Ralph, F. M., Das, T., Neiman, P. J., & Cayan, D. R. (2011). Atmospheric rivers, floods and the water resources of California. *Water*, *3*(2), 445–478. https://doi.org/10.3390/w3020445

Espinoza, V., Waliser, D. E., Guan, B., Lavers, D. A., & Ralph, F. M. (2018). Global analysis of climate change projection effects on atmospheric rivers. *Geophysical Research Letters*, *45*(9), 4299–4308. https://doi.org/10.1029/2017GL076968

Field, P. R., & Wood, R. (2007). Precipitation and cloud structure in midlatitude cyclones. *Journal of Climate*, *20*(2), 233–254. https://doi.org/10.1175/jcli3998.1

Gao, Y., Lu, J., Leung, R., Yang, Q., Hagos, S., & Qian, Y. (2015). Dynamical and thermodynamical modulations on future changes of landfalling atmospheric rivers over western North America. *Geophysical Research Letters*, *42*(17), 7179–7186. https://doi.org/10.1002/2015gl065435

Gershunov, A., Shulgina, T., Ralph, F. M., Lavers, D. A., & Rutz, J. J. (2017). Assessing the climate-scale variability of atmospheric rivers affecting western North America. *Geophysical Research Letters*, *44*(15), 7900–7908. https://doi.org/10.1002/2017gl074175

Gonzales, K. R., Swain, D. L., Barnes, E. A., & Diffenbaugh, N. S. (2020). Moisture-versus wind-dominated flavors of atmospheric rivers. *Geophysical Research Letters*, *47*(23), e2020GL090042. https://doi.org/10.1029/2020GL090042

Guan, B. (2021). Tracking atmospheric rivers globally as elongated targets (tARget), version 1 [Dataset]. https://doi.org/10.25346/S6/SJGRKY

Guan, B., Molotch, N. P., Waliser, D. E., Fetzer, E. J., & Neiman, P. J. (2010). Extreme snowfall events linked to atmospheric rivers and surface air temperature via satellite measurements. *Geophysical Research Letters*, *37*(20), L20401. https://doi.org/10.1029/2010gl044696

Guan, B., Molotch, N. P., Waliser, D. E., Fetzer, E. J., & Neiman, P. J. (2013). The 2010/2011 snow season in California's Sierra Nevada: Role of atmospheric rivers and modes of large-scale variability. *Water Resources Research*, *49*(10), 6731–6743. https://doi.org/10.1002/wrcr.20537

Guan, B., & Waliser, D. E. (2015). Detection of atmospheric rivers: Evaluation and application of an algorithm for global studies. *Journal of Geophysical Research: Atmospheres*, *120*(24), 12514–12535. https://doi.org/10.1002/2015jd024257

Guirguis, K., Gershunov, A., Shulgina, T., Clemesha, R. E. S., & Ralph, F. M. (2019). Atmospheric rivers impacting northern California and their modulation by a variable climate. *Climate Dynamics*, *52*(11), 6569–6583. https://doi.org/10.1007/s00382-018-4532-5

Guo, Y., Shinoda, T., Guan, B., Waliser, D. E., & Chang, E. K. M. (2020). Statistical relationship between atmospheric rivers and extratropical cyclones and anticyclones. *Journal of Climate*, *33*(18), 7817–7834. https://doi.org/10.1175/jcli-d-19-0126.1

Hersbach, H., Bell, B., Berrisford, P., Hirahara, S., Horányi, A., Muñoz-Sabater, J., et al. (2020). The ERA5 global reanalysis. *Quarterly Journal of the Royal Meteorological Society*, *146*(730), 1999–2049. https://doi.org/10.1002/qj.3803

Hu, H., & Dominguez, F. (2019). Understanding the role of tropical moisture in atmospheric rivers. *Journal of Geophysical Research: Atmospheres*, *124*(24), 13826–13842. https://doi.org/10.1029/2019jd030867

Inda-Díaz, H. A., O'Brien, T. A., Zhou, Y., & Collins, W. D. (2021). Constraining and characterizing the size of atmospheric rivers: A perspective independent from the detection algorithm. *Journal of Geophysical Research: Atmospheres*, *126*(16), e2020JD033746. https://doi.org/10.1029/2020JD033746

Jin, F.-F., Kim, S. T., & Bejarano, L. (2006). A coupled-stability index for ENSO. *Geophysical Research Letters*, *33*(23), L23708. https://doi.org/10.1029/2006GL027221

Kim, H., Zhou, Y., & Alexander, M. A. (2017). Changes in atmospheric rivers and moisture transport over the Northeast Pacific and western North America in response to ENSO diversity. *Climate Dynamics*, *52*(12), 1–14. https://doi.org/10.1007/s00382-017-3598-9

Kim, J., Waliser, D. E., Neiman, P. J., Guan, B., Ryoo, J. M., & Wick, G. A. (2013). Effects of atmospheric river landfalls on the cold season precipitation in California. *Climate Dynamics*, *40*(1–2), 465–474. https://doi.org/10.1007/s00382-012-1322-3

Knippertz, P., & Wernli, H. (2010). A Lagrangian climatology of tropical moisture exports to the Northern Hemispheric extratropics. *Journal of Climate*, *23*(4), 987–1003. https://doi.org/10.1175/2009jcli3333.1

Lavers, D. A., Allan, R. P., Villarini, G., Lloyd-Hughes, B., Brayshaw, D. J., & Wade, A. J. (2013). Future changes in atmospheric rivers and their implications for winter flooding in Britain. *Environmental Research Letters*, *8*(3), 034010. https://doi.org/10.1088/1748-9326/8/3/034010

Lavers, D. A., Allan, R. P., Wood, E. F., Villarini, G., Brayshaw, D. J., & Wade, A. J. (2011). Winter floods in Britain are connected to atmospheric rivers. *Geophysical Research Letters*, *38*(23), L23803. https://doi.org/10.1029/2011GL049783

Lavers, D. A., & Villarini, G. (2015). The contribution of atmospheric rivers to precipitation in Europe and the United States. *Journal of Hydrology*, *522*, 382–390. https://doi.org/10.1016/j.jhydrol.2014.12.010

Lavers, D. A., Villarini, G., Allan, R. P., Wood, E. F., & Wade, A. J. (2012). The detection of atmospheric rivers in atmospheric reanalyses and their links to British winter floods and the large-scale climatic circulation. *Journal of Geophysical Research*, *117*(D20), D20106. https://doi.org/10.1029/2012JD018027

Leung, L. R., Boos, W. R., Catto, J. L., DeMott, A. C., Martin, G. M., Neelin, J. D., et al. (2022). Exploratory precipitation metrics: Spatiotemporal characteristics, process-oriented, and phenomena-based. *Journal of Climate*, *35*(12), 3659–3686. https://doi.org/10.1175/jcli-d-21-0590.1

Lora, J. M., Shields, C. A., & Rutz, J. J. (2020). Consensus and disagreement in atmospheric river detection: ARTMIP global catalogues. *Geophysical Research Letters*, *47*(20), e2020GL089302. https://doi.org/10.1029/2020gl089302

McClenny, E. E., Ullrich, P. A., & Grotjahn, R. (2020). Sensitivity of atmospheric river vapor transport and precipitation to uniform sea-surface temperature increases. *Journal of Geophysical Research: Atmospheres*, *125*(21), e2020JD033421. https://doi.org/10.1029/2020jd033421

Mundhenk, B. D., Barnes, E. A., & Maloney, E. D. (2016). All-season climatology and variability of atmospheric river frequencies over the North Pacific. *Journal of Climate*, *29*(13), 4885–4903. https://doi.org/10.1175/Jcli-D-15-0655.1

Nash, D., Waliser, D., Guan, B., Ye, H., & Ralph, F. M. (2018). The role of atmospheric rivers in extratropical and polar hydroclimate. *Journal of Geophysical Research: Atmospheres*, *123*(13), 6804–6821. https://doi.org/10.1029/2017jd028130

Neiman, P. J., Ralph, F. M., Moore, B. J., Hughes, M., Mahoney, K. M., Cordeira, J. M., & Dettinger, M. D. (2013). The landfall and inland penetration of a flood-producing atmospheric river in Arizona. Part I: Observed synoptic-scale, orographic, and hydrometeorological characteristics. *Journal of Hydrometeorology*, *14*(2), 460–484. https://doi.org/10.1175/Jhm-D-12-0101.1

Neiman, P. J., Ralph, F. M., White, A. B., Kingsmill, D. E., & Persson, P. O. (2002). The statistical relationship between upslope flow and rainfall in California's coastal mountains: Observations during CALJET. *Monthly Weather Review*, *130*(6), 1468–1492. https://doi.org/10.1175/1520-0493(2002)130<1468:TSRBUF>2.0.CO;2

Neiman, P. J., Ralph, F. M., Wick, G. A., Lundquist, J. D., & Dettinger, M. D. (2008). Meteorological characteristics and overland precipitation impacts of atmospheric rivers affecting the West Coast of North America based on eight years of SSM/I satellite observations. *Journal of Hydrometeorology*, *9*(1), 22–47. https://doi.org/10.1175/2007jhm855.1

Newell, R. E., Newell, N. E., Zhu, Y., & Scott, C. (1992). Tropospheric rivers – A pilot-study. *Geophysical Research Letters*, *19*(24), 2401–2404. https://doi.org/10.1029/92gl02916

O'Brien, T. A., Payne, A. E., Shields, C. A., Rutz, J. J., Brands, S., Castellano, C., et al. (2020). Detection uncertainty matters for understanding atmospheric rivers. *Bulletin of the American Meteorological Society*, *101*(6), E790–E796. https://doi.org/10.1175/bams-d-19-0348.1

O'Brien, T. A., Risser, M. D., Loring, B., Elbashandy, A. A., Krishnan, H., Johnson, J., et al. (2020). Detection of atmospheric rivers with inline uncertainty quantification: TECA-BARD v1.0. *Geoscientific Model Development Discussions*, *2020*, 1–20. https://doi.org/10.5194/gmd-2020-55

Oueslati, B., Yiou, P., & Jézéquel, A. (2019). Revisiting the dynamic and thermodynamic processes driving the record-breaking January 2014 precipitation in the southern UK. *Scientific Reports*, *9*(1), 2859. https://doi.org/10.1038/s41598-019-39306-y

Papineau, J. M., & Holloway, E. (2011). The nature of heavy rain and flood events in Alaska. Retrieved from http://www.weather.gov

Patricola, C. M., O'Brien, J. P., Risser, M. D., Rhoades, A. M., O'Brien, T. A., Ullrich, P. A., et al. (2020). Maximizing ENSO as a source of western US hydroclimate predictability. *Climate Dynamics*, *54*(1–2), 351–372. https://doi.org/10.1007/s00382-019-05004-8

Payne, A. E., & Magnusdottir, G. (2014). Dynamics of landfalling atmospheric rivers over the North Pacific in 30 Years of MERRA reanalysis. *Journal of Climate*, *27*(18), 7133–7150. https://doi.org/10.1175/Jcli-D-14-00034.1

Payne, A. E., & Magnusdottir, G. (2015). An evaluation of atmospheric rivers over the North Pacific in CMIP5 and their response to warming under RCP 8.5. *Journal of Geophysical Research: Atmospheres*, *120*(21), 11173–11190. https://doi.org/10.1002/2015jd023586

Pfahl, S., & Sprenger, M. (2016). On the relationship between extratropical cyclone precipitation and intensity. *Geophysical Research Letters*, *43*(4), 1752–1758. https://doi.org/10.1002/2016GL068018

Prince, H. D., Gibson, P. B., DeFlorio, M. J., Corringham, T. W., Cobb, A., Guan, B., et al. (2021). Genesis Locations of the costliest atmospheric rivers impacting the Western United States. *Geophysical Research Letters*, *48*(20), e2021GL093947. https://doi.org/10.1029/2021GL093947

Ralph, F. M., Dettinger, M., Lavers, D., Gorodetskaya, I. V., Martin, A., Viale, M., et al. (2017). Atmospheric rivers emerge as a global science and applications focus. *Bulletin of the American Meteorological Society*, *98*(9), 1969–1973. https://doi.org/10.1175/bams-d-16-0262.1

Ralph, F. M., Neiman, P. J., & Rotunno, R. (2005). Dropsonde observations in low-level jets over the northeastern Pacific Ocean from CALJET-1998 and PACJET-2001: Mean vertical-profile and atmospheric-river characteristics. *Monthly Weather Review*, *133*(4), 889–910. https://doi.org/10.1175/Mwr2896.1

Ralph, F. M., Neiman, P. J., & Wick, G. A. (2004). Satellite and CALJET aircraft observations of atmospheric rivers over the eastern North Pacific Ocean during the winter of 1997/98. *Monthly Weather Review*, *132*(7), 1721–1745. https://doi.org/10.1175/1520-0493(2004)132<1721:Sacaoo>2.0.Co;2

Ralph, F. M., Rutz, J. J., Cordeira, J. M., Dettinger, M., Anderson, M., Reynolds, D., et al. (2019). A scale to characterize the strength and impacts of atmospheric rivers. *Bulletin of the American Meteorological Society*, *100*(2), 269–290. https://doi.org/10.1175/Bams-D-18-0023.1

Rutz, J. J., Shields, C. A., Lora, J. M., Payne, A. E., Guan, B., Ullrich, P., et al. (2019). The atmospheric river tracking method intercomparison project (ARTMIP): Quantifying uncertainties in atmospheric river climatology. *Journal of Geophysical Research: Atmospheres*, *124*(24), 13777–13802. https://doi.org/10.1029/2019jd030936

Rutz, J. J., Steenburgh, W. J., & Ralph, F. M. (2014). Climatological characteristics of atmospheric rivers and their inland penetration over the Western United States. *Monthly Weather Review*, *142*(2), 905–921. https://doi.org/10.1175/Mwr-D-13-00168.1

Ryoo, J. M., Kaspi, Y., Waugh, D. W., Kiladis, G. N., Waliser, D. E., Fetzer, E. J., & Kim, J. (2013). Impact of Rossby wave breaking on U.S. West Coast winter precipitation during ENSO events. *Journal of Climate*, *26*(17), 6360–6382. https://doi.org/10.1175/Jcli-D-12-00297.1

Shields, C. A., Rutz, J. J., Leung, L. Y., Ralph, F. M., Wehner, M., Kawzenuk, B., et al. (2018). Atmospheric river tracking method intercomparison project (ARTMIP): Project goals and experimental design. *Geoscientific Model Development*, *11*(6), 2455–2474. https://doi.org/10.5194/gmd-11-2455-2018

Smith, B. L., Yuter, S. E., Neiman, P. J., & Kingsmill, D. E. (2010). Water vapor fluxes and orographic precipitation over Northern California associated with a landfalling atmospheric river. *Monthly Weather Review*, *138*(1), 74–100. https://doi.org/10.1175/2009mwr2939.1

Sodemann, H., & Stohl, A. (2013). Moisture origin and meridional transport in atmospheric rivers and their association with multiple cyclones. *Monthly Weather Review*, *141*(8), 2850–2868. https://doi.org/10.1175/Mwr-D-12-00256.1

Waliser, D. E., & Guan, B. (2017). Extreme winds and precipitation during landfall of atmospheric rivers. *Nature Geoscience*, *10*(3), 179–U183. https://doi.org/10.1038/Ngeo2894

Warner, M. D., Mass, C. F., & Salathe, E. P. (2015). Changes in winter atmospheric rivers along the North American West Coast in CMIP5 climate models. *Journal of Hydrometeorology*, *16*(1), 118–128. https://doi.org/10.1175/Jhm-D-14-0080.1

21698996, 2022, 23, Downloaded from https://agupubs.onlinelibrary.wiley.com/doi/10.1029/2022JD037105, Wiley Online Library on [06/06/2023]. See the Terms and Conditions (https://onlinelibrary.wiley.com/terms-and-conditions) on Wiley Online Library for rules of use; OA articles are governed by the applicable Creative Commons License

Williams, I. N., & Patricola, C. M. (2018). Diversity of ENSO events unified by convective threshold sea surface temperature: A nonlinear ENSO index. *Geophysical Research Letters*, *45*(17), 9236–9244. https://doi.org/10.1029/2018gl079203

Xiong, Y., & Ren, X. (2021). Influences of atmospheric rivers on North Pacific winter precipitation: Climatology and dependence on ENSO condition. *Journal of Climate*, *34*(1), 277–292. https://doi.org/10.1175/JCLI-D-20-0301.1

Yettella, V., & Kay, J. E. (2016). How will precipitation change in extratropical cyclones as the planet warms? Insights from a large initial condition climate model ensemble. *Climate Dynamics*, *49*(5–6), 1765–1781. https://doi.org/10.1007/s00382-016-3410-2

Zavadoff, B. L., & Kirtman, B. P. (2020). Dynamic and thermodynamic modulators of European atmospheric rivers. *Journal of Climate*, *33*(10), 4167–4185. https://doi.org/10.1175/jcli-d-19-0601.1

Zhang, Z., Ralph, F. M., & Zheng, M. (2019). The relationship between extratropical cyclone strength and atmospheric river intensity and position. *Geophysical Research Letters*, *46*(3), 1814–1823. https://doi.org/10.1029/2018gl079071

Zhou, Y., & Kim, H. (2019). Impact of distinct origin locations on the life cycles of landfalling atmospheric rivers over the U.S. West Coast. *Journal of Geophysical Research: Atmospheres*, *124*(22), 11897–11909. https://doi.org/10.1029/2019jd031218

Zhou, Y., Kim, H., & Guan, B. (2018). Life cycle of atmospheric rivers: Identification and climatological characteristics. *Journal of Geophysical Research: Atmospheres*, *123*(22), 12715–12725. https://doi.org/10.1029/2018JD029180

Zhou, Y., O'Brien, T. A., Collins, W. D., Shields, C. A., Loring, B., & Elbashandy, A. A. (2022). Data for "Characteristics and variability of winter northern Pacific atmospheric river flavors" [Dataset]. https://doi.org/10.5281/zenodo.6998797

Zhou, Y., O'Brien, T. A., Ullrich, P. A., Collins, W. D., Patricola, C. M., & Rhoades, A. M. (2021). Uncertainties in atmospheric river lifecycles by detection algorithms: Climatology and variability. *Journal of Geophysical Research: Atmospheres*, *126*(8), e2020JD033711. https://doi.org/10.1029/2020jd033711

Zhu, Y., & Newell, R. E. (1994). Atmospheric rivers and bombs. *Geophysical Research Letters*, *21*(18), 1999–2002. https://doi.org/10.1029/94GL01710

21698996, 2022, 23, Downloaded from https://agupubs.onlinelibrary.wiley.com/doi/10.1029/2022JD037105, Wiley Online Library on [06/06/2023]. See the Terms and Conditions (https://onlinelibrary.wiley.com/terms-and-conditions) on Wiley Online Library for rules of use; OA articles are governed by the applicable Creative Commons License